HHS Public Access

Author manuscript

Sci Transl Med. Author manuscript; available in PMC 2016 July 15.

Published in final edited form as:

Sci Transl Med. 2015 July 15; 7(296): 296ra110. doi:10.1126/scitranslmed.aaa8791.

Plasticity of the human visual system after retinal gene therapy in patients with Leber's congenital amaurosis

Manzar Ashtari[1,2,*], **Hui Zhang**[3], **Philip A. Cook**[4], **Laura L. Cyckowski**[5], **Kenneth S. Shindler**[1,2], **Kathleen A. Marshall**[1,6], **Puya Aravand**[1,2], **Arastoo Vossough**[5], **James C. Gee**[4], **Albert M. Maguire**[1,2], **Chris I. Baker**[7], and **Jean Bennett**[1,2]

[1]F.M. Kirby Center for Molecular Ophthalmology, Scheie Eye Institute, Department of Ophthalmology, University of Pennsylvania, Philadelphia, PA 19014, USA

[2]Center for Advanced Retinal and Ocular Therapeutics, University of Pennsylvania Perelman School of Medicine, 309 Stellar-Chance Labs, 422 Curie Boulevard, Philadelphia, PA 19104, USA

[3]Department of Computer Science, University College London, Gower Street, London WC1E 6BT, UK

[4]Penn Image Computing and Science Laboratory, Department of Radiology, University of Pennsylvania, 3600 Market Street, Philadelphia, PA 19104, USA

[5]Department of Radiology, The Children's Hospital of Philadelphia, Philadelphia, PA 19014, USA

[6]Center for Cellular and Molecular Therapeutics at The Children's Hospital of Philadelphia, Colket Translational Research Building, 3501 Civic Center Boulevard, Philadelphia, PA 19014, USA

[7]Laboratory of Brain and Cognition, National Institutes of Health, 10 Center Drive, MSC 1240, Bethesda, MD 20892, USA

Abstract

Much of our knowledge of the mechanisms underlying plasticity in the visual cortex in response to visual impairment, vision restoration, and environmental interactions comes from animal studies.

[*]Corresponding author: ashtari@chop.edu.

SUPPLEMENTARY MATERIALS

www.sciencetranslationalmedicine.org/cgi/content/full/7/296/296ra110/DC1

Materials and Methods

Table S1. Demographic summary for LCA2 patients including clinical data for visual acuity and visual fields at the time of MRI.

References (51–56)

Author contributions: M.A., J.B., H.Z., P.A.C., L.L.C., C.I.B., K.A.M., K.S.S., J.C.G., and A.V. participated in the acquisition and/or analysis of data. M.A., J.B., H.Z., L.L.S., C.I.B., K.S.S., P.A.C., J.C.G., and A.V. participated in the design and/or interpretation of the reported experiments or results. A.M.M., J.B., K.A.M., M.A., and L.L.C. carried out the clinical, and research procedures. M.A., J.B., and L.L.C. obtained regulatory approvals. M.A., J.B., C.I.B., H.Z., K.S.S., P.A., and J.C.G. participated in drafting and/or revising the manuscript. M.A. wrote the manuscript, and all other authors reviewed and edited the intermediate and final versions of the manuscript.

Competing interests: J.B. and A.M.M. are co-inventors on a U.S. patent (no. 8,147,823) for a method to treat or slow the development of blindness, but both waived any financial interest in this technology in 2002. J.B. serves on the scientific advisory board for Avalanche Technologies and served on the scientific advisory board for Sanofi-Aventis (2010 to 2011). J.B. has consulted for GlaxoSmithKline. J.B. and A.M.M. are running clinical trials that are sponsored by Spark Therapeutics. J.B. is a founder of GenSight Biologics. The other authors declare that they have no competing interest.

We evaluated human brain plasticity in a group of patients with Leber's congenital amaurosis (LCA), who regained vision through gene therapy. Using non-invasive multimodal neuroimaging methods, we demonstrated that reversing blindness with gene therapy promoted long-term structural plasticity in the visual pathways emanating from the treated retina of LCA patients. The data revealed improvements and normalization along the visual fibers corresponding to the site of retinal injection of the gene therapy vector carrying the therapeutic gene in the treated eye compared to the visual pathway for the untreated eye of LCA patients. After gene therapy, the primary visual pathways (for example, geniculostriate fibers) in the treated retina were similar to those of sighted control subjects, whereas the primary visual pathways of the untreated retina continued to deteriorate. Our results suggest that visual experience, enhanced by gene therapy, may be responsible for the reorganization and maturation of synaptic connectivity in the visual pathways of the treated eye in LCA patients. The interactions between the eye and the brain enabled improved and sustained long-term visual function in patients with LCA after gene therapy.

INTRODUCTION

Much of our knowledge of plasticity in the human visual system comes from studies investigating the impact of sensory input deprivation. For example, studies of blind individuals have suggested recruitment of the visual cortex for nonvisual tasks such as reading Braille (1) or even verbal memory (2). However, there are limited studies (primarily single case studies) regarding the effects on plasticity after the enhancement of visual input (3, 4).

Numerous animal studies have reported structural changes in visual pathways after the implementation of visual deprivation. For example, dark-reared mice or rats have reduced quantities of spines in the pyramidal cells of the primary visual cortex (V1), potentially due to loss of visual inputs (5, 6). Similarly, unilateral eye closure in animals, as first demonstrated in cats by Hubel and Wiesel (7), produces a marked reduction in arborization of the geniculostriate fibers, which serve the deprived eye and terminate in layer 4 of the visual cortex. Subsequent studies of unilateral eye closure further confirmed these initial observations and the remarkable remodeling of the geniculostriate fibers due to visual deprivation (8, 9). Recently, Yu *et al*. (10) conducted a longitudinal study that tracked visual responses and changes in dendritic spines in the ferret visual cortex after brief periods of unilateral eye closure. Similar to earlier reports (10), improved visual function in the deprived eye was tightly correlated with structural alterations in V1. Parallel to the shrinkage in arborization of neurons in V1 and geniculostriate fibers, most unilateral eye closure studies have also reported an increase in the synaptic terminals serving the open eye (8, 10, 11). Together, these animal studies demonstrate that visual deprivation leads to a reorganization of the dendritic architecture of V1 cortical neurons. Similar structural changes with visual deprivation have also been reported in studies of humans blind from birth or shortly thereafter, including apparent atrophy of the geniculostriate tracts (12) and reduction in the volume (13) and fractional anisotropy (14) of the splenium of the corpus callosum. Thus, it is important to ascertain if the structural changes caused by lack of vision are reversible when vision is restored.

In an attempt to answer this question, many animal experiments first induced unilateral eye closure and then reversed the process, restoring visual input. Results from these studies have consistently demonstrated that both the structural and functional changes induced by unilateral eye closure are largely reversible when the deprived eye is reopened. The most common features of this structural reversibility have been reported to be within the lateral geniculate nucleus (LGN), V1, or along the geniculostriate fibers. For example, Dürsteler *et al*. (15) showed a partial regrowth of geniculate cells receiving projections from the deprived eye only a few days after reversing eyelid suture in kittens. In monkeys, recovery of geniculostriate arbors was shown in layer 4 of V1 after reverse suture during the critical period of development after birth (16, 17). In agreement with these aforementioned reports, Movshon and Blakemore (18), in a study of reverse eyelid suture in kittens, demonstrated that geniculostriate fibers exhibit a shift in favor of the open eye 10 days after an initial week of monocular deprivation. Finally, a recent study of unilateral eye closure and reversal of suturing in ferrets (10) reported the recovery from unilateral eye closure to be rapid and robust, occurring within a few hours of eye opening, and that as little as 24 hours after eye opening, dendritic spines could return to the same numbers as before unilateral eye closure (10).

Whereas all the animal studies highlighted so far elucidate the specific neuronal underpinnings responsible for changes in visual cortex in response to visual impairment, vision restoration, and environment interactions, similar studies have not been possible in humans because of the invasiveness of the procedures. With access to a group of genotypically and phenotypically characterized subjects with Leber’s congenital amaurosis type 2 (LCA2), who underwent gene therapy and gained some visual function, we had a unique opportunity to draw parallels between cortical plasticity changes reported in animal studies with reverse eyelid suture (with sight restoration) and human retinal gene therapy in LCA2 patients (with sight restoration).

Distinct from the eyelid suture animal studies where vision is typically restored to the entirety of the retina, the clinical trial of gene therapy in LCA2 patients restored vision to specific regions of the retina based on the site of injection of the viral vector carrying the therapeutic gene. As different parts of the retina feed visual inputs to the brain via distinct visual pathways, this presents an opportunity to separately examine structural and functional changes of these pathways due to continued visual deprivation (untreated retina of patients) and restoration (treated retina of patients). For example, the temporal fibers of the retina signal to the ipsilateral visual cortex, whereas the nasal fibers cross to the contralateral hemisphere. Thus, subretinal injection to the temporal area of the retina may restore visual input to the ipsilateral V1 through the ipsilateral geniculostriate fibers, whereas injection into the nasal area of the retina may restore visual input to the contralateral V1.

Comparing treated and untreated eyes within the same patient, we previously demonstrated the efficacy of gene therapy for treating LCA2 as shown by measurements of retinal and visual function as well as functional magnetic resonance imaging (fMRI). Both the retina and visual cortex were much more sensitive to light stimulation in the treated eye as compared to the untreated eye, even after prolonged (up to 44 years) visual deprivation of both eyes (19). Although the enhanced responsiveness of the visual cortex is suggestive of

plasticity, it could simply reflect the engagement of maintained visual pathways after restoration of input. In the current study, we set out to ascertain the role of structural brain plasticity by investigating the impact of visual deprivation and subsequent vision restoration (by gene therapy) on the major visual pathways in patients with LCA2, and how these changes related to alterations in the structural properties of the visual cortex.

We used diffusion tensor imaging (DTI) to examine the effect of deprivation and subsequent unilateral retinal gene therapy on the organization and/or reorganization of white matter microstructure in V1, and we used DTI tractography to examine the effect of deprivation and unilateral gene therapy on the integrity and/or plasticity of white matter fiber bundles connecting V1 to the primary and higher-order visual centers in the brain. Finally, cortical activation induced by stimulation of the treated eye in LCA2 patients and the corresponding eye in sighted controls was compared to evaluate functional outcomes resulting from gene therapy.

RESULTS

Participants in the neuroimaging study included 10 LCA2 patients (6 males) and 11 demographically matched sighted controls (8 males). Control subjects were matched for age, gender, ethnicity, and handedness. LCA2 patients received unilateral gene therapy to their worse-seeing eye. In the absence of baseline imaging data (before gene therapy), the untreated eye was used as a control in addition to comparing the data for treated and untreated retina to that for sighted controls. Table 1 summarizes the characteristics of LCA2 patients and demographically matched sighted controls.

Our initial analyses focused on group differences between LCA2 patients and sighted controls using both voxel-based analyses of diffusion parameters and averaged fractional anisotropy values relative to the principle diffusion direction of the white matter tracts connecting the occipital lobes to other brain areas (tractography). Diffusion results were then correlated with age (reflecting the progression of the disease) and clinical symptoms. All but 1 of the LCA2 patients received their subretinal injection to the right eye, and all 10 subjects received their injection in the superior temporal aspect of the macula/retina. Because projections from the right superior temporal retina remain ipsilateral and do not cross over in the optic chiasm, then retinal gene therapy should predominantly affect the visual pathways projecting to the right hemisphere. Thus, comparing the diffusion results of the left hemisphere between LCA2 patients and controls could reveal the effect of continued deprivation on the structural properties of the visual pathways. In contrast, comparing the diffusion results of the left and right visual pathways within LCA2 patients provided a measure of the impact of retinal gene therapy.

The white matter microstructure in the primary visual cortex of LCA2 patients is compromised

Results of voxel-based analysis for fractional anisotropy of LCA2 patients compared with the sighted control group revealed a number of clusters of reduced fractional anisotropy within both the right and left occipital lobes (Fig. 1A, column 1, yellow clusters). Reduced fractional anisotropy clusters were superimposed onto the color fractional anisotropy

population-based atlas constructed from all study participants (n = 21). As shown in the axial views of Fig. 1A, reduced fractional anisotropy clusters were located bilaterally in the occipital cortex with larger clusters in the left (3272 voxels) compared to the right (2301 voxels) hemisphere. A χ^2 test of these counts revealed a highly significant difference (χ^2 = 169.2, $P < 0.001$) from a symmetrical distribution. Reduced fractional anisotropy clusters were mainly situated in the vicinity of the calcarine fissure [Brodmann area (BA) 17 and 18)] and are clearly shown on the sagittal image of Fig. 1A (white arrows). An additional reduced fractional anisotropy cluster for LCA2 patients was found in the splenium of the corpus callosum (Fig. 1B). This location is known to be involved in binocular vision, and through this location pass fiber bundles (occipital-callosal fibers) connecting the left and right occipital cortices (20). Voxel-based analyses did not reveal any clusters with increased fractional anisotropy at the same statistical threshold (see Fig. 1 legend).

Water diffusivity relative to the principle diffusion direction of the fibers is called axial diffusivity; the component of diffusivity relative to the direction perpendicular to the principal direction is called radial diffusivity; and the measure of the average diffusivity in all directions is called mean diffusivity (see DTI voxel-based analysis). LCA2 patients showed clusters of increased radial diffusivity (Fig. 1A, column 2, blue clusters). Similar to the fractional anisotropy results, increased radial diffusivity clusters were also primarily located in the medial aspect of the visual cortex and distributed in and around the calcarine fissures (i.e., V1). LCA2 patients also showed increased mean diffusivity (Fig. 1A, column 3, blue clusters), again bilaterally distributed and medially located in the visual cortex near the calcarine fissure. Finally, analysis of axial diffusivity did not reveal significant clusters of abnormality for the LCA2 patients as compared to the sighted control group. Collectively, voxel-based analyses for the primary diffusion indices of fractional anisotropy, radial diffusivity, and mean diffusivity for LCA2 patients as compared to sighted controls suggested compromised white matter microstructures for LCA2 patients in bilateral primary visual cortices (V1 areas) with stronger effects in the left compared to the right hemisphere (Fig. 1A) and the splenium of the corpus callosum. Table 2 presents detailed information on coordinates, cluster size, and locations in the Montreal Neurological Institute (MNI) template (http://neuro.debian.net/pkgs/fsl-atlases.html) along with their Brodmann Area (BA) for all diffusion parameters (fractional anisotropy, radial diffusivity, and mean diffusivity) obtained from the voxel-based analysis of the LCA2 group compared with the sighted controls. The mean and standard deviation (SD) of the average diffusion parameters for clusters in the left and right visual cortices are shown in Table 3.

Previous reports from animal and human studies (21, 22) have shown that a combination of decreased fractional anisotropy and increased radial diffusivity and mean diffusivity (Table 3) without significant changes in axial diffusivity may be indicative of demyelination or reduced/arrested myelination.

Voxel-based analyses additionally revealed that the compromised white matter microstructures showed a distinct asymmetric pattern. In particular, as shown in Table 3, LCA2 patients presented with lower fractional anisotropy and higher radial diffusivity and mean diffusivity values for the left as compared to their right visual cortex, whereas diffusion parameters for sighted controls were roughly similar for both occipital cortices. It

is important to note that we included all patients (9 of 10 treated in the right eye and 1 of 10 treated in the left eye) in the group analysis, comparing LCA2 patients with demographically matched controls. Although the group voxel-based analyses results showed more compromised white matter in the left, for the one subject who received subretinal injection in the left eye, diffusion results were completely reversed. As shown in Table 3, average fractional anisotropy for the right occipital cortex was 0.260 for controls and 0.202 for LCA2 patients with no significant difference. On the other hand, the right occipital fractional anisotropy value for the one subject treated in the left eye was 0.18, which is lower than the values of fractional anisotropy reported for both the LCA2 and control groups. Similarly, the values for the left occipital fractional anisotropy were 0.252 for controls and 0.199 (Table 3) for LCA2 patients, whereas the fractional anisotropy value for the left occipital cortex for the one subject treated in the left eye was 0.23, demonstrating a clearly reversed pattern of asymmetry in this patient. In Table 3, the diffusion values appear close for the left and right occipital cortex but differ significantly from a statistical perspective. This is because the asymmetries in each individual are masked in the average of the values from all individuals due to the wide age range and spectrum of disease severity in our subjects (see Fig. 2).

In an additional analysis, the average fractional anisotropy values from two regions of interest in the V1 (calcarine area) of both hemispheres were compared between the LCA2 patients and controls, revealing significant differences between the left and right regions of interest in the LCA2 patients, but not controls, and a significant difference between the two groups for the left region of interest only ($P < 0.017$). The region-of-interest analyses showed left average fractional anisotropy values of 0.129 and 0.161 for the LCA2 and controls, respectively ($P < 0.017$). Results for the average fractional anisotropy of the right region of interest were 0.142 for LCA2 patients and 0.168 for controls ($P > 0.23$). Notably, the left and right mean fractional anisotropy for the calcarine regions of interest of the one subject injected in the left eye were 0.166 (left) and 0.142 (right), respectively. Similar to the voxel-based analyses results, the region-of-interest results also showed an increased fractional anisotropy within the visual cortex ipsilateral to the treated eye. Lower values for fractional anisotropy for this region-of-interest analysis are due to higher concentration of gray matter in the calcarine area.

These observed asymmetries may be because unilateral ocular gene therapy (in the temporal retina of the right eye in nine subjects and temporal retina of the left eye in one subject) predominantly affected the visual pathways projecting to the ipsilateral hemisphere of the treated eye and not the fibers crossing to the contralateral side. This asymmetry in voxel-based analyses for LCA2 patients was closely examined in the whole group by further performing tractography and analyzing white matter integrity along the left and right fiber tracts terminating in the occipital cortex.

Our results are consistent with reports in humans with early or congenital blindness (12–14, 23–25) that found significant disruptive white matter changes especially in the V1 when compared with matched sighted controls. The above voxel-based analyses and region-of-interest analyses clearly demonstrate a reverse normalization process for the occipital microstructural white matter for patients treated in the right eye versus the one subject

treated in the left eye. Further tractography and correlational analyses were focused only on the 9 of 10 subjects treated in the right eye to ensure unbiased statistical results.

White matter integrity of the primary visual cortex correlates with age

LCA is known to occur bilaterally, affecting both eyes (26, 27), and thus the disease should similarly affect both visual cortices. LCA is a degenerative disease (27, 28) and, even though there was variability because each individual in our study (except for a twin pair) had different *RPE65* mutations and each had different environmental exposures, age could be considered a proxy for disease progression. A case report showing a clear correlation between degree of retinal/visual function in an LCA2 patient and age supports this premise (29). As such, separate Spearman correlations were performed between the age and the average fractional anisotropy (from the significant clusters with reduced fractional anisotropy) of the left and right occipital cortices (Fig. 2). No correlations between fractional anisotropy and age were observed for the left ($R = 0.10$, $P < 0.770$) or right ($R = 0.155$, $P < 0.650$) occipital clusters for the control subjects. This developmental trajectory of the occipital fractional anisotropy with age for control subjects, as shown in Fig. 2, is consistent with previous reports. For example, examining age-related changes for fractional anisotropy in various brain regions, Salat *et al*. (30) and Davatzikos and Resnick (31) reported that occipital fibers are myelinated at an early age and are relatively preserved over time. Although LCA2 patients demonstrated a similar absence of correlation with age for their right occipital fractional anisotropy ($R = -0.467$, $P < 0.25$), their left occipital fractional anisotropy showed a negative correlation with age ($R = -0.633$, $P < 0.067$) (Fig. 2). A direct comparison of groups showed a trend for differences in correlation between the two groups for the left but not right occipital fractional anisotropy (Fisher test, $P < 0.058$ and $P > 0.10$, respectively). The asymmetry in the correlations of fractional anisotropy with age (albeit a trend that did not reach significance) is consistent with the asymmetry observed in the voxel-based analyses results (Fig. 1A). The decline of the occipital fractional anisotropy with age may be attributed to the degenerative nature of LCA2 disease, which in turn would lead to further disuse of the visual cortex over time.

The age-related changes of fractional anisotropy for the posterior corpus callosum in both LCA2 (left panel) and sighted controls (right panel) are shown in the bottom panels of Fig. 2. Control subjects presented significant positive correlations between posterior corpus callosum and age ($R = 0.70$, $P < 0.029$), which is consistent with reports on the fractional anisotropy of the corpus callosum and its positive correlation with age for normal aging subjects (32). However, the LCA2 patients showed no correlation with age for this region ($R = -0.167$, $P < 0.67$), but did show deviation in their microstructural white matter development over their life-span trajectory. Direct comparison between groups showed that the difference in correlation for the posterior corpus callosum fractional anisotropy was significant ($P < 0.028$).

In summary, age correlations with fractional anisotropy in sighted controls are consistent with previous reports on the occipital cortex (30, 31) and corpus callosum (32). The correlation results for LCA2 patients are suggestive of greater effects of gene therapy on the

right visual cortex (V1) as compared to the left, a trend that is consistent with the results of voxel-based analyses (Fig. 1).

Gene therapy enhances the integrity of white matter microstructure in the visual cortex of LCA2 patients

To further examine the effect of retinal gene therapy on white matter microstructure of the visual cortex, we performed correlational analysis between the average fractional anisotropy values of the right and left voxel-based analyses–reported clusters of diffusion abnormalities (Tables 2 and 3) as a function of the amount of time between the administration of gene therapy and the MRI scans (9 of 10 patients). As shown in Fig. 3, the left fractional anisotropy values depict significant negative correlations with time after gene therapy, whereas the fractional anisotropy values for the right visual cortex are not negatively correlated. They show a trend toward improvement (slight positive slope) with time after intervention. Furthermore, there was a significant difference between the left and right occipital fractional anisotropy with respect to their correlation with treatment time ($P < 0.003$, Steiger's test for dependent correlations) (33). These results show strong asymmetry in the values of the right and left white matter microstructures of the visual cortex, a finding consistent with aforementioned correlations of fractional anisotropy and age.

Amplitude and frequency of nystagmus correlates with compromised white matter microstructure of the left visual cortex

Exploratory Spearman partial correlations (covaried for age) were performed to evaluate possible relationships between the reduced fractional anisotropy clusters within the left and right occipital cortices and several clinical measures including visual acuity, visual field, full-field sensitivity, and amplitude and frequency of nystagmus (9 of 10 patients). The only clinical symptoms that significantly correlated with fractional anisotropy values (Bonferroni corrected $q = 0.05/14 = 0.0036$) were the frequency and amplitude of nystagmus for both eyes (Fig. 4). In particular, the left occipital fractional anisotropy values showed significant correlations with amplitude of nystagmus in the right ($R = -0.98$, $P = 0.002$) and left ($R = -0.92$, $P = 0.01$) eyes, as well as the frequency of nystagmus in both the right ($R = -0.96$, $P = 0.002$) and left eyes ($R = -0.95$, $P = 0.004$).

Fiber tractography reveals asymmetric disrupted geniculostriate connectivity in visual pathways of LCA2 patients

Collectively, results from animal studies (10, 15–17) and early blind human studies (12) report effects of visual deprivation and its reversal in the LGN, V1, and geniculostriate fibers. To examine the effects of long-term deprivation and restoration of vision on the geniculostriate tracts (connecting LGN to V1) as well as other fibers connecting the occipital cortex to the rest of the brain in LCA2 patients, we conducted diffusion fiber tractography (see Diffusion tensor tractography). The average fractional anisotropy along the left and right white matter fiber bundles terminating in the occipital cortex (including inferior longitudinal fasciculus, occipito-callosal, and inferior fronto-occipital fasciculus, as well as optic chiasm fibers) was assessed. Assessment was also carried out for the corticospinal tracts that do not terminate in the occipital cortex. These were viewed as control fibers.

Extracted tracts for inferior fronto-occipital fasciculus, inferior longitudinal fasciculus, occipito-callosal, geniculostriate, optic chiasm, and corticospinal tract fibers are presented in Fig. 5A. Tractography analyses of all of these tracts showed no difference between the LCA2 patients and sighted controls, except for the geniculostriate fibers (Table 4; Bonferroni corrected $\alpha = 0.05/12 = 0.0042$). To investigate the effects on the geniculostriate fibers more closely, we conducted analysis of variance (ANOVA) using hemisphere as a repeated measures factor, group as a between-subjects factor, and age as a covariate. This analysis revealed a significant main effect of group ($P < 0.042$) as well as a significant interaction between group and hemisphere ($P < 0.044$). Further, as shown in Table 4, post hoc *t* tests revealed significant differences between groups for the left ($P < 0.0045$) but not the right geniculostriate fibers ($P > 0.389$). These results confirm a specific difference between patients and controls for the untreated side (Table 4). We further computed a laterality index [(right geniculostriate average fractional anisotropy − left geniculostriate average fractional anisotropy)/(right geniculostriate average fractional anisotropy + left geniculostriate average fractional anisotropy)] of the averaged fractional anisotropy along the right and left geniculostriate fibers between the LCA2 patients and the demographically matched controls (Fig. 5B), demonstrating a significantly ($P < 0.04$) larger laterality index in the LCA2 patients as compared to matched sighted controls. Tractography results also suggested that all other extracted cortico-cortical connections between the visual cortex and the rest of the brain were well preserved in the LCA2 patients, as no differences were observed compared to the demographically matched controls.

In summary, tractography results were consistent with voxel-based analyses and Spearman correlations of fractional anisotropy with age. On the basis of voxel-based analyses, tractography, and age correlation, results suggested a normalization process within V1 and geniculostriate fibers of the right hemisphere initiated by gene therapy in the superior temporal macula/retina of the right eye. To further test this hypothesis, we next examined the existence and degree of functional asymmetry of the visual cortex in response to gene therapy as compared to the distribution of cortical activation observed in sighted controls.

LCA2 patients show similar asymmetry in visual cortical activation patterns as observed in geniculostriate connectivity

The structural MRI data presented above suggested that gene therapy applied to the temporal retina of the right eye reversed structural injury in the right geniculostriate fibers that was caused by visual deprivation. To examine whether functional brain responses followed the structural changes brought about by gene therapy and show a similar normalization along the right geniculostriate tract, a retrospective analysis was performed to compare fMRI results of nine LCA2 patients treated in the right eye to the average responses from the right eye of the nine matched sighted controls. Figure 6A shows the group-averaged fMRI results from the right eye of matched controls, demonstrating a near symmetrical hemispheric activation distribution in response to the checkerboard paradigm (19, 34). This is expected from the connectivity of the human retina to the brain (35), with each eye connected roughly equally to both hemispheres (53% of axons crossing the optic chiasm and 47% staying ipsilateral). In contrast, group-averaged fMRI results for the LCA2 patients (treated in the right eye), as shown in Fig. 6B, depicted significantly larger cortical activation in the right

hemisphere as compared to the left hemisphere in response to the same visual stimulus. This asymmetry of cortical activations in LCA2 patients (R > L) followed a similar pattern of asymmetry as observed for the averaged fractional anisotropy values along the geniculostriate fibers (R > L). To further quantify this asymmetry, the volume of cortical activation distributed over the entire right and left visual cortices was calculated for both the LCA2 patients and sighted control subjects (Table 5). A laterality index was then obtained: (right total # of activated voxels − left total # of activated voxels)/(right total # of activated voxels + left total # of activated voxels). As depicted in Fig. 6C, the laterality index for total visual cortex activation induced by stimulation of the right eye in LCA2 patients and matched sighted control subjects using the same high-contrast checkerboard stimuli was significantly greater for the LCA2 patients ($P < 0.003$).

DISCUSSION

Human LCA2 patients treated with subretinal gene therapy have experienced significant and prolonged improvements in vision over time. These improvements have been mostly attributed to the rescued retinal cells, but vision develops from the joint collaboration between the eye and the brain. Focusing on a group of visually impaired LCA2 patients who had received unilateral temporal retinal gene therapy (in their worse-seeing eye), we report evidence for structural plasticity in the visual pathways ipsilateral to the treated retina. First, consistent with previous reports in animal (5, 6, 8, 11, 15, 16, 36) and blind human studies (12, 24, 37), we found impaired structural properties of the visual pathways compared with matched sighted controls, suggesting atrophy of the visual pathways after extended visual deprivation. Critically, however, these structural differences were asymmetric, with reduced differences between the LCA2 patients (9 of 10 treated in the right eye) and sighted controls in the right occipital cortex compared with the left, corresponding closely with the projections from the site of sub-retinal gene vector administration. Furthermore, for the one subject who received treatment to the left eye, this effect was reversed with the left occipital cortex showing normalization. This group structural asymmetry was observed in voxel-based analyses, tractography, and correlational analyses, and was further supported by an asymmetry in the functional responses of the visual cortex. Collectively, our findings suggest that restoration of retinal function may lead to strengthening of the visual projections into the cortex. The types of structural changes seen in our current study are similar to those reported in recent findings on the relationship between the integrity of white matter tracts of the visual system and cortical function in a group of patients with compression of the optic chiasm by pituitary gland tumors and recovery of visual abilities after surgical removal of the tumor and subsequent decompression of the visual fibers (38). These authors showed that compression of the optic chiasm led to demyelination of the optic tracts, and the severity of demyelination in patients predicted visual ability and functional activity of the primary visual areas. Furthermore, subsequent to decompression of optic chiasm, rapid regeneration of myelin in the human brain was observed, which was closely correlated with cortical visual activities, and ultimately the recovery of patients' visual function (38). Results from this study are highly relevant to the current report as the authors clearly demonstrate human brain plasticity depicted by the remyelination process of the

visual fibers and a direct relationship between the degree of remyelination and the visual ability of the patients.

Although the optimal neuroimaging study design for the evaluation of the effects of gene therapy on the human brain would be to capture the baseline brain state before any intervention (for example, gene therapy), our neuroimaging protocol was conducted independently from the LCA2 clinical trial and started after the LCA2 trial had been initiated. Thus, we did not have access to these patients at baseline (before gene therapy). This is a limitation of the current study, but by comparing functional and structural differences between the treated and untreated eyes, our data reveal important insights into brain plasticity after restoration of vision.

Similar to the results reported by Paul *et al*. (38), the structural and functional changes we observed could be due to increased myelination of V1 and geniculostriate fibers, which in the case of gene therapy are thought to depend on life experiences and environmental interactions (39). For example, Ishibashi *et al*. (40) reported that repeated electrical stimulation of axons results in an increase in myelination. More recently, considerable structural plasticity was reported in the brains of gorillas living in a naturalistic environment as compared to those who were caged. Also, living in different habitats with seminaturalistic environments alters brain structure in adult marmosets (41). Not only did animals living in more complex environments have more connections between neurons, but they also exhibited a higher rate of neurogenesis than their caged control counterparts. Consistent with these reports, our results demonstrate that reversing blindness through gene therapy, and the subsequent increase in visual experiences and interactions with the environment, promotes long-term structural plasticity, which in turn further enhances visual function (see structural and functional asymmetry indices, Figs. 4C and 5C, respectively). Although vision results from a collaborative effort between the eye and the brain, the degree of the brain's involvement in securing long-term preservation and improvement of what was initiated by retinal gene delivery has not yet been carefully examined and deserves closer investigation. Evidence for changes in white matter structure through training has been reported in other cross-sectional and longitudinal studies in humans. For example, Bengtsson *et al*. (42) reported differences in the spino-thalamic tract between musicians and nonmusicians. Similarly, changes in white matter structure have been reported in subjects training to juggle (43) or performing a balancing task (44) over several weeks. Thus, it is plausible that LCA2 patients involved in future retinal gene therapy studies may benefit from exercises designed to enhance the use and function of the visual pathway.

The major limitation of the current study is lack of access to the baseline brain state of LCA2 patitents before any intervention (for example, gene therapy). This limitation was due to the fact that the neuroimaging study component was conducted independently from the LCA2 clinical trial and started after the LCA2 trial had been initiated. Despite this limitation, by comparing functional and structural differences between the treated and untreated eyes, the data reveal important insights into brain plasticity after restoration of vision. Another constraint is the limited correlations observed for the white matter integrity value of fractional anisotropy and patients' clinical symptoms. Although white matter microstructural abnormalities showed correlations with nystagmus, no correlations were

detected for principal visual parameters such as visual acuity and visual field. Inclusion of participants with ages ranging from 11 to 47 years may be an additional limitation when studying white matter due to normal developmental processes across a wide age span. However, as reflected by our results presented here and by other data reported by Salat *et al*. (30) and Davatzikos and Resnick (31), occipital fibers are myelinated at an early age and are relatively preserved over time.

In conclusion, results from DTI, diffusion tractography, and fMRI along with correlation of these data with nystagmus measures, age, and length of time after treatment in LCA2 patients suggested that retinal gene therapy may indeed promote remyelination of geniculostriate fiber axons as well as local changes within the V1 favoring the treated eye. These observations also suggest that the functional plasticity that we previously reported for LCA2 patients receiving retinal gene therapy (19, 34) may be related to structural changes in the brain. Thus, retinal gene therapy and structural remodeling of the V1 and geniculostriate fibers may indeed be joint processes that are necessary to sustain long-term restoration of visual function. However, longitudinal neuroimaging studies capturing the baseline brain state (before gene therapy) are also essential to broaden our knowledge of the effects that retinal gene therapy (or cell therapy) may have on the human visual cortex or the central nervous system. Such a longitudinal design will also shed light on timing of the plasticity process.

MATERIALS AND METHODS

Study design

We designed a neuroimaging study for 10 LCA2 patients previously treated in a clinical trial to evaluate the safety and efficacy of retinal gene augmentation therapy. Eligibility requirements included prior participation in a retinal gene therapy trial involving unilateral (single eye) gene augmentation therapy. Structural and functional images of participants' brains were obtained on a 3-T magnet using 30-direction isotropic (1.7 mm in *x*, *y*, and *z* directions) DTI and fMRI methodology. Using DTI, integrity of the microstructural white matter was assessed between unilaterally treated LCA2 patients and a group of demographically matched sighted controls. Applying fiber tractography, white matter fiber bundles connecting the visual cortex to other brain regions were extracted and compared among LCA2 patients and sighted controls. Clinical measures were correlated with microstructural abnormalities identified among LCA2 patients. The visual responses of patients and controls were measured using fMRI while presenting visual stimuli (black and white reversing checkerboards) to the left and right eye separately. Cortical responses from the left and right hemispheres were compared among the patients and controls by quantifying activated areas of the occipital cortex to assess the effect of retinal gene therapy on the human visual system.

Leber's congenital amaurosis

LCA is a rare retinal degenerative blinding disease, usually inherited in an autosomally recessive fashion, with no available treatment or cure. It is symptomatic at birth or in the first few months of life, and affects about 1 in 81,000 people (45). LCA has been associated

with mutations in at least 18 different genes. Mutations in the gene encoding retinal pigment epithelium-specific protein *65 kD* (*RPE65*) are involved in one of the more common forms of LCA, LCA2. LCA2 patients are good candidates for gene therapy because the degeneration of their retinal cells is slow, thus increasing the probability of successful gene transfer to the remaining (although sickly) retinal cells. There are several active clinical trials evaluating gene augmentation therapy for LCA2 patients (www.clinicaltrials.gov), and our subjects had been enrolled in study NCT00516477.

Study participants

Participants in the clinical trial consisted of 12 LCA2 patients, including adults, many of whom had more advanced retinal disease than did the pediatric participants (4 of 12 were pediatric participants) (46, 47). One of the U.S. Food and Drug Administration (FDA) mandates for the phase 1 clinical trial was for gene therapy to be administered in the patients' worse-seeing eye. As such, comprehensive psychophysical examinations were performed to identify and document the worse-seeing eye in all clinical trial patients. Other subjects were initially enrolled to protect children from the unforeseen complications of the first retinal gene therapy clinical trial using AAV2-hRPE65v2. The initial subjects enrolled were three adults (46). After the demonstration of safety and efficacy of gene therapy in this group, additional subjects, including four children, received the intervention. However, still the worse-seeing eye was treated in light of potential risk/benefit ratios. In the current manuscript, we present the neuroimaging evaluation from 10 of 12 LCA2 patients enrolled in the phase 1 clinical trial. Comprehensive clinical evaluation of all patients determined the worse-seeing eye to be the right eye for 9 of 10 patients and the left eye for 1 of 10 patients. The patients (six males) received subretinal injection of AAV2-hRPE65v2 (46, 47) in the worse-seeing eye ≥ 2 years before their MRI study. Eleven sighted control subjects who were demographically matched (eight males) were recruited by flyers and word of mouth. Controls were excluded if they had any current or past psychiatric diagnosis or a history of drug or alcohol abuse. Additional exclusion criteria for all subjects included mental retardation, known neurological disorders, a history of head injury or any focal findings revealed by MRI, or current use of psychotropic medications. Table 1 summarizes the overall characteristics for matching of LCA2 patients and controls.

Gene therapy

A summary of information regarding the LCA2 patients, gene mutation, age, gender, site of injections, as well as their clinical visual testing for visual acuity and visual fields are presented in table S1. Detailed information about the clinical presentations of these patients who were evaluated as part of the phase 1 LCA2 clinical trial is presented elsewhere (47). In summary, all 12 patients who received unilateral gene therapy showed improvement in at least one measure of their retinal function. Most of the patients showed sustained improvement in several assessments of their retinal/visual functions such as light sensitivity, pupillometry, visual acuity, nystagmus, and ambulation (47). When patients were tested for their ability to navigate a standardized obstacle course before administration of *AAV2-hRPE65v2*, 11 of 12 patients had great difficulty, particularly in dim light. After injection, subjects (especially children) showed substantial improvement in their ambulation when using their injected eye only (47). The LCA2 patients had bilaterally diminished light

sensitivity and pupillary light reflexes at baseline, and they showed improvements in these parameters after gene therapy in their treated eye. One subject gained nearly the same level of light sensitivity as that in age-matched normal controls (47). The success rate for recovery and magnitude of improvement was related to the age at treatment, with best results obtained in children.

From the 10 participants in our neuroimaging study, two patients received the low dose (1.5×10^{10} vector genomes), six had the medium dose (4.8×10^{10} vector genomes), and two were injected with the high dose (1.5×10^{11} vector genomes) of the *AAV2-hRPE65v2* virus (47). Nine of 10 patients received their subretinal injections to the right eye and one to the left eye. All injections were administered primarily into the superior temporal aspect of the macula (47). This is important because the specific site in the retina chosen for vector delivery can play a key role in understanding the subsequent effects that retinal gene therapy may have in particular locations of the visual pathway.

Informed consent (or parental permission and child assent) was obtained from all subjects for the institutional review board–approved gene therapy clinical trial. These individuals were consented separately for the neuroimaging study, as were control subjects. All control subjects were initially screened by phone and subsequently invited to participate in the study. Subjects were excluded from the neuroimaging study if they had a positive pregnancy test, expressed claustrophobia, had a metallic implanted prosthetic or device (for example, cardiac pacemaker) or other contraindications for MRI, had excessive metallic dental work (including braces and nonremovable retainers), or were noncompliant. LCA2 subjects had to meet strict inclusion/exclusion criteria to be invited to participate in the gene therapy trial (46, 47). None of the subjects had a history of drug/alcohol abuse. All individuals that were recruited had very close family support and provided extensive history, including prescription drugs, over-the-counter medications, and food/drink habits. Although there was no formal psychiatric screening carried out, each individual was interviewed in depth by several members of the study team to determine whether they could comply with the heavy time commitment and whether they had the concentration necessary to carry out all of the testing at baseline and follow-up visits.

Magnetic resonance imaging

MRI scans were conducted at the Children's Hospital of Philadelphia on a research-dedicated 3T Siemens Verio system using a 32-channel head coil. All scans were carried out by a single operator and monitored to be free of artifacts at the time of acquisition. Details of image acquisition and processing for structural and functional neuroimaging are presented in the Supplementary Materials.

DTI voxel-based analysis—Before voxel-based analysis, diffusion tensor volumes were spatially normalized using PipeDream (http://brianavants.wordpress.com/software/). The normalized tensor volumes were then used to compute scalar images for fractional anisotropy, radial diffusivity [$\lambda\perp = (\lambda 2 + \lambda 3)/2$], axial diffusivity ($\lambda\| = \lambda 1$), and mean diffusivity [$D = (\lambda 1 + \lambda 2 + \lambda 3)/3$] (48). The normalized scalar images were smoothed with a 6-mm Gaussian kernel [in three dimensions (3D)]. To limit the analysis to primarily white

matter brain areas, a conservative white matter mask was computed to exclude cortical and subcortical gray matter and cerebral spinal fluid. The mask was constructed by averaging the normalized fractional anisotropy images of all subjects and subsequently thresholded to retain only the major white matter bundles. The same mask was used for the voxel-based analysis. Statistical analyses were performed using the MRIcron software (www.mccauslandcenter.sc.edu/mricro/), which uses a permuted Brunner-Munzel (BM) rank-order statistic (49). BM (50) is also known as the generalized Wilcoxon test and is more appropriate than the *t* test for data that are not normally distributed. Diffusion data in the current study did not follow a normal distribution; thus, BM was used for all data analyses. Comparisons were conducted across all the voxels in the entire brain volume. To correct for multiple comparisons, we used the FDR and a corrected (α) level of $q < 0.05$. As an additional safeguard against false positives, we only retained clusters of size greater than 100 voxels for all analyses. To provide a common reference for our findings, we have further registered the population-based template, and thresholded fractional anisotropy, radial diffusivity, and axial diffusivity images to the MNI template to report the locations of the significant clusters in the MNI coordinates along with BAs (http://noodle.med.yale.edu/~papad/mni2tal/).

Diffusion tensor tractography—Methodological details of fiber tractography are presented in the Supplementary Materials. Major fiber tracts connecting the visual cortex to the rest of the brain and forming part of the visual pathways, such as geniculostriate fibers, inferior longitudinal fasciculus, inferior fronto-occipital fasciculus, optic chiasm, and occipito-callosal fibers, as well as a set of control fibers that are not related to vision such as corticospinal tracts, were extracted to examine whether regaining sight, due to gene therapy, would have an effect on these fiber tracts. After extraction, the tract-specific fibers were superimposed as an anatomical region of interest onto the normalized fractional anisotropy images for each subject to obtain the average fractional anisotropy of each tract for individual subjects in both LCA2 and sighted control groups.

fMRI visual stimuli—In the past, using simple contrast reversing checkerboard stimuli, we demonstrated efficacy of gene therapy in this patient population (19, 34). Similar to our earlier study, the fMRI paradigm consisted of 15-s blocks of flickering (8-Hz) black and white checkerboards, which consisted of three contrasts of high, medium, and low, interleaved with 15 s of blank (black) screens (19, 34). Subjects were asked to fixate on a yellow cross in the center of the checkerboard patterns, or, if they could not see the cross, were asked to look straight ahead. Resonance Technology VisuaStim (www.mrivideo.com) goggles featuring a digital display and a 30° horizontal field of view was used to present the fMRI stimuli. The visual paradigm was programmed in E-Prime (www.pstnet.com/eprime.cfm).

Statistical analyses

All voxel-based analyses of DTI data were performed using the MRI-cron software (www.mccauslandcenter.sc.edu/mricro/), which uses a permuted BM rank-order statistic (49). BM (50) is also known as the generalized Wilcoxon test and is more appropriate than the *t* test for data that are not normally distributed. All fMRI data were processed using a

general linear model corrected for multiple comparison using FDR as implemented in BrainVoyager QX (www.brainvoyager.com). Participant's demographic characteristics, imaging data, and clinical measurements were summarized by standard descriptive summaries (for example, mean and SD for continuous variables such as age, fractional anisotropy, and radial diffusivity; mean diffusivity and percentages for categorical variables such as gender and grouping categories). Graphical displays of the data were used to assess distributional assumptions. Nonparametric approaches such as the Spearman rank correlation coefficient (ρ) and the Mann-Whitney test for comparison of two groups were considered. Two-group *t* tests were used to compare means of continuous measures, and Fisher exact tests were used for comparison of proportions between LCA2 patients and controls. Linear regression was applied to adjust comparisons between groups for additional variables (for example, age). For exploratory analyses, Bonferroni correction was applied as noted in the main text. Statistical analyses were conducted using SPSS v21 with a two-sided *P* value <0.05 as the criterion for statistical significance except for planned comparisons.

Supplementary Material

Refer to Web version on PubMed Central for supplementary material.

Acknowledgments

We thank T. Feirweier of Siemens for providing us with the diffusion sequence, and J. Rundio, P. Lam, R. Golembski, and J. Dell for their expert technical assistance.

Funding: Funding was provided by the NIH R21EY020662, Foundation Fighting Blindness–sponsored CHOP-PENN (The Children's Hospital of Philadelphia–Penn Medicine) Pediatric Center for Retinal Degenerations, C-GT-0913-06280UPA03, NIH 8DP1EY023177, NIH 1R24EY019861, Transdisciplinary Awards Program in Translational Medicine and Therapeutics (TAPITMAT) grants, University of Pennsylvania, Research to Prevent Blindness, and the F.M. Kirby Foundation. C.I.B. is supported by the Intramural Research Program of the National Institute of Mental Health.

REFERENCES AND NOTES

1. Sadato N, Pascual-Leone A, Grafman J, Ibañez V, Deiber MP, Dold G, Hallett M. Activation of the primary visual cortex by Braille reading in blind subjects. Nature. 1996; 380:526–528. [PubMed: 8606771]
2. Burton H, Snyder AZ, Diamond JB, Raichle ME. Adaptive changes in early and late blind: A fMRI study of verb generation to heard nouns. J Neurophysiol. 2002; 88:3359–3371. [PubMed: 12466452]
3. Fine I, Wade AR, Brewer AA, May MG, Goodman DF, Boynton GM, Wandell BA, MacLeod DI. Long-term deprivation affects visual perception and cortex. Nat Neurosci. 2003; 6:915–916. [PubMed: 12937420]
4. Valvo, A.; Clark, LL.; Jastrzembska, ZS. Sight Restoration After Long Term Blindness: The Problems and Behavior Patterns of Visual Rehabilitation. American Foundation for the Blind; New York: 1971.
5. Valverde F. Apical dendritic spines of the visual cortex and light deprivation in the mouse. Exp Brain Res. 1967; 3:337–352. [PubMed: 6031165]
6. Borges S, Berry M. The effects of dark rearing on the development of the visual cortex of the rat. J Comp Neurol. 1978; 180:277–300. [PubMed: 659662]
7. Hubel DH, Wiesel TN. Receptive fields, binocular interaction and functional architecture in the cat's visual cortex. J Physiol. 1962; 160:106–154. [PubMed: 14449617]

8. Antonini A, Stryker MP. Development of individual geniculocortical arbors in cat striate cortex and effects of binocular impulse blockade. J Neurosci. 1993; 13:3549–3573. [PubMed: 8340819]
9. Antonini A, Fagiolini M, Stryker MP. Anatomical correlates of functional plasticity in mouse visual cortex. J Neurosci. 1999; 19:4388–4406. [PubMed: 10341241]
10. Yu H, Majewska AK, Sur M. Rapid experience-dependent plasticity of synapse function and structure in ferret visual cortex in vivo. Proc Natl Acad Sci USA. 2011; 108:21235–21240. [PubMed: 22160713]
11. Wiesel TN, Hubel DH. Single-cell responses in striate cortex of kittens deprived of vision in one eye. J Neurophysiol. 1963; 26:1003–1017. [PubMed: 14084161]
12. Shimony JS, Burton H, Epstein AA, McLaren DG, Sun SW, Snyder AZ. Diffusion tensor imaging reveals white matter reorganization in early blind humans. Cereb Cortex. 2006; 16:1653–1661. [PubMed: 16400157]
13. Yu C, Shu N, Li J, Qin W, Jiang T, Li K. Plasticity of the corticospinal tract in early blindness revealed by quantitative analysis of fractional anisotropy based on diffusion tensor tractography. Neuroimage. 2007; 36:411–417. [PubMed: 17442594]
14. Leporé N, Voss P, Lepore F, Chou YY, Fortin M, Gougoux F, Lee AD, Brun C, Lassonde M, Madsen SK, Toga AW, Thompson PM. Brain structure changes visualized in early- and late-onset blind subjects. Neuroimage. 2010; 49:134–140. [PubMed: 19643183]
15. Dürsteler MR, Garey LJ, Movshon JA. Reversal of the morphological effects of monocular deprivation in the kittens's lateral geniculate nucleus. J Physiol. 1976; 261:189–210. [PubMed: 994029]
16. LeVay S, Wiesel TN, Hubel DH. The development of ocular dominance columns in normal and visually deprived monkeys. J Comp Neurol. 1980; 191:1–51. [PubMed: 6772696]
17. Swindale NV, Vital-Durand F, Blakemore C. Recovery from monocular deprivation in the monkey. III. Reversal of anatomical effects in the visual cortex. Proc R Soc Lond Ser B. 1981; 213:435–450. [PubMed: 6119690]
18. Movshon JA. Reversal of the physiological effects of monocular deprivation in the kitten's visual cortex. J Physiol. 1976; 261:125–174. [PubMed: 994027]
19. Ashtari M, Cyckowski LL, Monroe JF, Marshall KA, Chung DC, Auricchio A, Simonelli F, Leroy BP, Maguire AM, Shindler KS, Bennett J. The human visual cortex responds to gene therapy–mediated recovery of retinal function. J Clin Invest. 2011; 121:2160–2168. [PubMed: 21606598]
20. Dougherty RF, Ben-Shachar M, Bammer R, Brewer AA, Wandell BA. Functional organization of human occipital-callosal fiber tracts. Proc Natl Acad Sci USA. 2005; 102:7350–7355. [PubMed: 15883384]
21. Song SK, Yoshino J, Le TQ, Lin SJ, Sun SW, Cross AH, Armstrong RC. Demyelination increases radial diffusivity in corpus callosum of mouse brain. Neuroimage. 2005; 26:132–140. [PubMed: 15862213]
22. Tyszka JM, Readhead C, Bearer EL, Pautler RG, Jacobs RE. Statistical diffusion tensor histology reveals regional dysmyelination effects in the shiverer mouse mutant. Neuroimage. 2006; 29:1058–1065. [PubMed: 16213163]
23. Shu N, Liu Y, Li J, Li Y, Yu C, Jiang T. Altered anatomical network in early blindness revealed by diffusion tensor tractography. PLOS One. 2009; 4:e7228. [PubMed: 19784379]
24. Noppeney U, Friston KJ, Ashburner J, Frackowiak R, Price CJ. Early visual deprivation induces structural plasticity in gray and white matter. Curr Biol. 2005; 15:R488–R490. [PubMed: 16005276]
25. Ptito M, Schneider FC, Paulson OB, Kupers R. Alterations of the visual pathways in congenital blindness. Exp Brain Res. 2008; 187:41–49. [PubMed: 18224306]
26. Yannuzzi LA. Central serous chorioretinopathy: A personal perspective. Am J Ophthalmol. 2010; 149:361–363. [PubMed: 20172062]
27. Chung DC, Traboulsi EI. Leber congenital amaurosis: Clinical correlations with genotypes, gene therapy trials update, and future directions. J AAPOS. 2009; 13:587–592. [PubMed: 20006823]
28. Perrault I, Rozet JM, Gerber S, Ghazi I, Leowski C, Ducroq D, Souied E, Dufier JL, Munnich A, Kaplan J. Leber congenital amaurosis. Mol Genet Metab. 1999; 68:200–208. [PubMed: 10527670]

29. Al-Khayer K, Hagstrom S, Pauer G, Zegarra H, Sears J, Traboulsi EI. Thirty-year follow-up of a patient with leber congenital amaurosis and novel RPE65 mutations. Am J Ophthalmol. 2004; 137:375–377. [PubMed: 14962443]
30. Salat DH, Smith EE, Tuch DS, Benner T, Pappu V, Schwab KM, Gurol ME, Rosas HD, Rosand J, Greenberg SM. White matter alterations in cerebral amyloid angiopathy measured by diffusion tensor imaging. Stroke. 2006; 37:1759–1764. [PubMed: 16763176]
31. Davatzikos C, Resnick SM. Degenerative age changes in white matter connectivity visualized in vivo using magnetic resonance imaging. Cereb Cortex. 2002; 12:767–771. [PubMed: 12050088]
32. Kochunov P, Williamson DE, Lancaster J, Fox P, Cornell J, Blangero J, Glahn DC. Fractional anisotropy of water diffusion in cerebral white matter across the lifespan. Neurobiol Aging. 2012; 33:9–20. [PubMed: 20122755]
33. Steiger JH. Tests for comparing elements of a correlation matrix. Psychol Bull. 1980; 87:245–251.
34. Bennett J, Ashtari M, Wellman J, Marshall KA, Cyckowski LL, Chung DC, McCague S, Pierce EA, Chen Y, Bennicelli JL, Zhu X, Ying GS, Sun J, Wright JF, Auricchio A, Simonelli F, Shindler KS, Mingozzi F, High KA, Maguire AM. AAV2 gene therapy readministration in three adults with congenital blindness. Sci Transl Med. 2012; 4:120ra115.
35. Hertle, RW.; Dell'Osso, LF. Nystagmus in Infancy and Childhood: Current Concepts in Mechanisms, Diagnoses, and Management. Oxford Univ. Press; New York: 2013.
36. Hubel DH, Wiesel TN. The period of susceptibility to the physiological effects of unilateral eye closure in kittens. J Physiol. 1970; 206:419–436. [PubMed: 5498493]
37. Pan WJ, Wu G, Li CX, Lin F, Sun J, Lei H. Progressive atrophy in the optic pathway and visual cortex of early blind Chinese adults: A voxel-based morphometry magnetic resonance imaging study. Neuroimage. 2007; 37:212–220. [PubMed: 17560797]
38. Paul DA, Gaffin-Cahn E, Hintz EB, Adeclat GJ, Zhu T, Williams ZR, Vates GE, Mahon BZ. White matter changes linked to visual recovery after nerve decompression. Sci Transl Med. 2014; 6:266ra173.
39. Fields RD. White matter in learning, cognition and psychiatric disorders. Trends Neurosci. 2008; 31:361–370. [PubMed: 18538868]
40. Ishibashi T, Dakin KA, Stevens B, Lee PR, Kozlov SV, Stewart CL, Fields RD. Astrocytes promote myelination in response to electrical impulses. Neuron. 2006; 49:823–832. [PubMed: 16543131]
41. Kozorovitskiy Y, Gross CG, Kopil C, Battaglia L, McBreen M, Stranahan AM, Gould E. Experience induces structural and biochemical changes in the adult primate brain. Proc Natl Acad Sci USA. 2005; 102:17478–17482. [PubMed: 16299105]
42. Bengtsson SL, Nagy Z, Skare S, Forsman L, Forssberg H, Ullén F. Extensive piano practicing has regionally specific effects on white matter development. Nat Neurosci. 2005; 8:1148–1150. [PubMed: 16116456]
43. Scholz J, Klein MC, Behrens TE, Johansen-Berg H. Training induces changes in white-matter architecture. Nat Neurosci. 2009; 12:1370–1371. [PubMed: 19820707]
44. Taubert M, Draganski B, Anwander A, Müller K, Horstmann A, Villringer A, Ragert P. Dynamic properties of human brain structure: Learning-related changes in cortical areas and associated fiber connections. J Neurosci. 2010; 30:11670–11677. [PubMed: 20810887]
45. Stone EM. Leber congenital amaurosis—A model for efficient genetic testing of heterogeneous disorders: LXIV Edward Jackson memorial lecture. Am J Ophthalmol. 2007; 144:791–811. [PubMed: 17964524]
46. Maguire AM, Simonelli F, Pierce EA, Pugh EN Jr, Mingozzi F, Bennicelli J, Banfi S, Marshall KA, Testa F, Surace EM, Rossi S, Lyubarsky A, Arruda VR, Konkle B, Stone E, Sun J, Jacobs J, Dell'Osso L, Hertle R, Ma J-X, Redmond TM, Zhu X, Hauck B, Zelenaia O, Shindler KS, Maguire MG, Wright JF, Volpe NJ, McDonnell JW, Auricchio A, High KA, Bennett J. Safety and efficacy of gene transfer for Leber's congenital amaurosis. N Engl J Med. 2008; 358:2240–2248. [PubMed: 18441370]
47. Maguire AM, High KA, Auricchio A, Wright JF, Pierce EA, Testa F, Mingozzi F, Bennicelli JL, Ying GS, Rossi S, Fulton A, Marshall KA, Banfi S, Chung DC, Morgan JI, Hauck B, Zelenaia O, Zhu X, Raffini L, Coppieters F, De Baere E, Shindler KS, Volpe NJ, Surace EM, Acerra C,

Lyubarsky A, Redmond TM, Stone E, Sun J, McDonnell JW, Leroy BP, Simonelli F, Bennett J. Age-dependent effects of RPE65 gene therapy for Leber's congenital amaurosis: A phase 1 dose-escalation trial. Lancet. 2009; 374:1597–1605. [PubMed: 19854499]

48. Pierpaoli C, Basser PJ. Toward a quantitative assessment of diffusion anisotropy. Magn Reson Med. 1996; 36:893–906. [PubMed: 8946355]
49. Nichols TE, Holmes AP. Nonparametric permutation tests for functional neuroimaging: A primer with examples. Hum Brain Mapp. 2002; 15:1–25. [PubMed: 11747097]
50. Brunner E, Munzel U. The nonparametric Behrens-Fisher problem: Asymptotic theory and a small-sample approximation. Biom J. 2000; 42:17–25.
51. Zhang H, Yushkevich PA, Alexander DC, Gee JC. Deformable registration of diffusion tensor MR images with explicit orientation optimization. Med Image Anal. 2006; 10:764–785. [PubMed: 16899392]
52. Zhang H, Yushkevich PA, Rueckert D, Gee JC. Unbiased white matter atlas construction using diffusion tensor images. Med Image Comput Comput Assist Interv. 2007; 10:211–218. [PubMed: 18044571]
53. Mori S, Kaufmann WE, Davatzikos C, Stieltjes B, Amodei L, Fredericksen K, Pearlson GD, Melhem ER, Solaiyappan M, Raymond GV, Moser HW, van Zijl PC. Imaging cortical association tracts in the human brain using diffusion-tensor-based axonal tracking. Magn Reson Med. 2002; 47:215–223. [PubMed: 11810663]
54. Okada T, Miki Y, Fushimi Y, Hanakawa T, Kanagaki M, Yamamoto A, Urayama S, Fukuyama H, Hiraoka M, Togashi K. Diffusion-tensor fiber tractography: Intraindividual comparison of 3.0-T and 1.5-T MR imaging. Radiology. 2006; 238:668–678. [PubMed: 16396839]
55. Wakana S, Jiang H, Nagae-Poetscher LM, van Zijl PC, Mori S. Fiber tract–based atlas of human white matter anatomy. Radiology. 2004; 230:77–87. [PubMed: 14645885]
56. Ashtari M, Cyckowski L, Yazdi A, Viands A, Marshall K, Bókkon I, Maguire A, Bennett J. fMRI of retina-originated phosphenes experienced by patients with Leber congenital amaurosis. PLOS One. 2014; 9:e86068. [PubMed: 24465873]

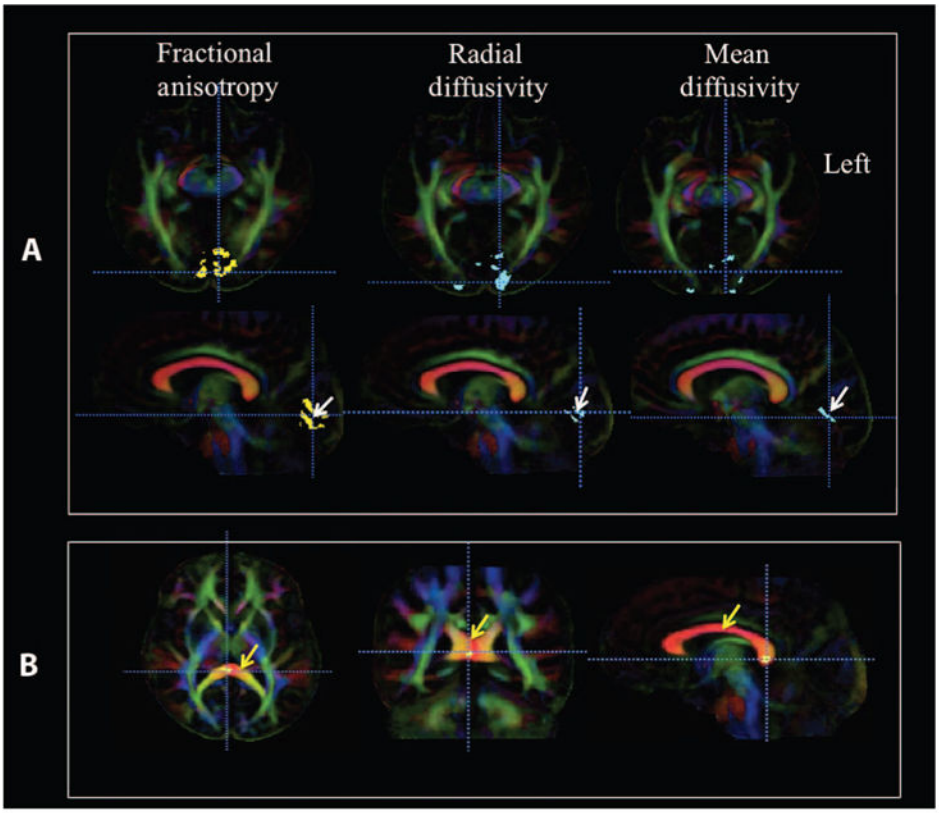

Fig. 1. Voxel-based analyses of diffusion maps comparing LCA2 patients with sighted controls

(**A**) Voxel-based analyses of LCA2 patients versus demographically matched normal sighted controls are shown for three diffusion parameters: fractional anisotropy, radial diffusivity, and mean diffusivity. Voxel-based analyses are superimposed onto the color fractional anisotropy population-based atlas constructed from all study participants (n = 21). Images of color fractional anisotropy are presented in the radiological convention (left brain is depicted on the right). In the first column, the voxel-based analyses for fractional anisotropy (revealed as yellow areas; white arrow on sagittal image, second row) showed decreased fractional anisotropy for greater than 100 contiguous voxels, which is significant after correction for multiple comparisons [false discovery rate (FDR), $q < 0.05$]. Axial images (top row, first column) show larger clusters with reduced fractional anisotropy in the left V1 (3272 voxels) as compared to the right V1 (2301 voxels). Sagittal images (second row, first column) are presented to demonstrate that the reduced fractional anisotropy clusters within the visual cortex are primarily located in and around the calcarine fissure (white arrow), which is also known as the primary visual area (BA-17 and BA-18). In the second column, results from voxel-based analyses for increased radial diffusivity are shown (at the same statistical threshold for fractional anisotropy) in blue clusters superimposed onto the color fractional anisotropy atlas. Similar to fractional anisotropy, the radial diffusivity clusters are larger in the left occipital cortex and primarily located in V1. In the third column, voxel-based analyses for increased mean diffusivity are also shown in blue clusters at the same statistical threshold for fractional anisotropy and radial diffusivity. The increase in mean diffusivity is not as widespread as the radial diffusivity and fractional anisotropy. This may

be because no changes in axial diffusivity were detected. (**B**) Reduced fractional anisotropy clusters (at the same statistical threshold) in the posterior corpus callosum (corpus callosum is marked with yellow arrows) where the left and right occipital fibers that connect the two visual cortices cross. No changes in other diffusion indices were detected for the corpus callosum cluster.

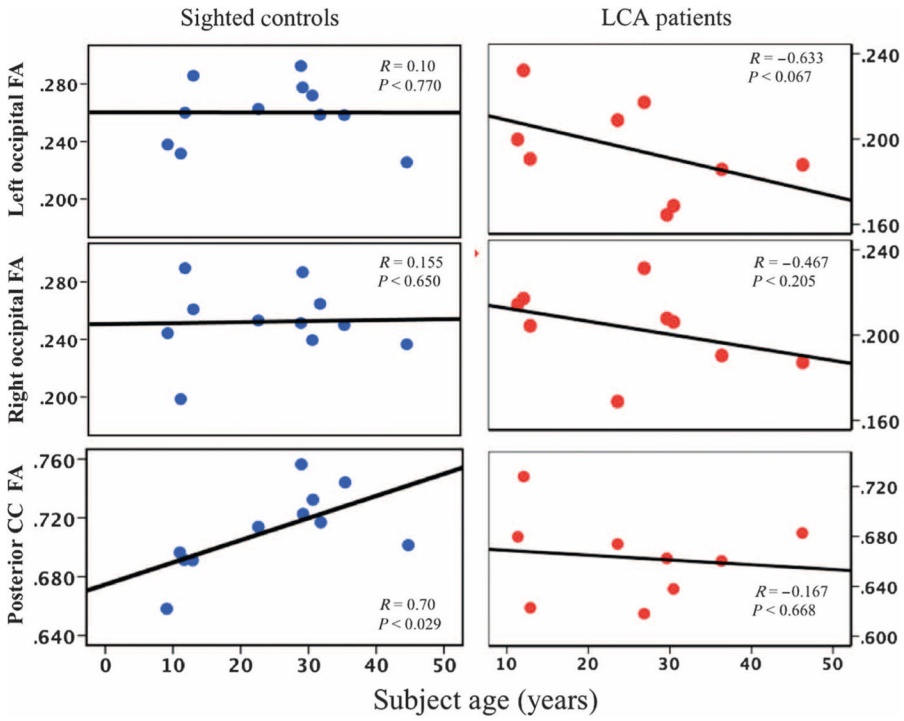

Fig. 2. Spearman correlations for occipital fractional anisotropy with age in LCA2 patients and sighted controls

Shown are Spearman correlation analyses for white matter microstructural abnormalities within the right and left occipital cortex and posterior corpus callosum (CC) with age for LCA2 patients and sighted controls. LCA2 patients demonstrated similar correlations to those for sighted controls for the right occipital fractional anisotropy (FA), but the left occipital fractional anisotropy negatively correlated with age, thus demonstrating a continuous decline of the microstructural white matter in the left primary visual area for these patients. However, the posterior corpus callosum fractional anisotropy correlations with age were noticeably different for LCA2 patients compared to sighted controls. The absence of positive correlations for fractional anisotropy and patients' age in the splenium of the corpus callosum for LCA2 patients may be due to the progressive nature of the disease, signifying the decline in communication between the two visual cortices over time and the reduction in the number of fibers crossing the splenium, which connects the left and right occipital cortices and enables binocular vision.

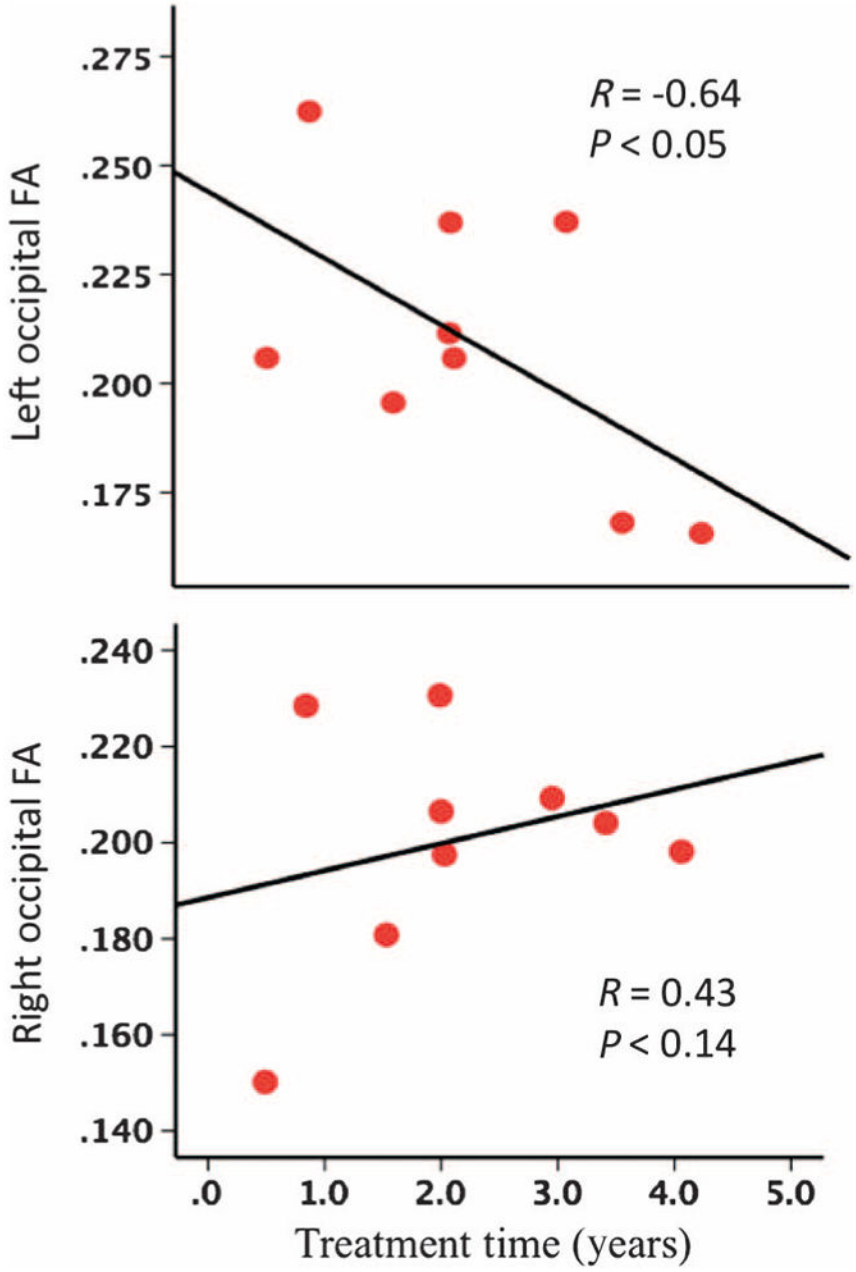

Fig. 3. Spearman correlations for the left and right occipital fractional anisotropy and time since gene therapy

The left and right occipital FA correlated with the number of years after gene therapy for LCA2 patients treated in their right eye at the time of the MRI scan. Results show significant negative correlations ($R = -0.64$, $P < 0.05$) for the left occipital fractional anisotropy and a trend (but not significant) toward a positive correlation ($R = 0.43$, $P < 0.14$) for the right occipital fractional anisotropy and time since gene therapy. There was a significant difference between the left and right occipital fractional anisotropy with respect to correlation with time since gene therapy ($P < 0.003$, Steiger's test for dependent correlations) (33).

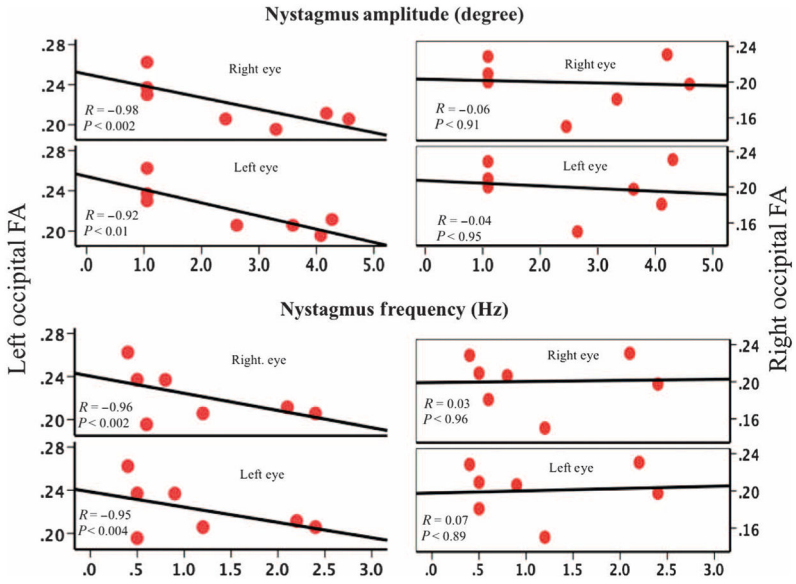

Fig. 4. Spearman correlations for occipital fractional anisotropy and the amplitude and frequency of nystagmus in LCA2 patients

Correlations for the left and right occipital FA and the frequency and amplitude of nystagmus for the left and right eye of LCA2 patients are shown. Nystagmus characteristics for either the right or the left eye did not correlate with the integrity of white matter microstructure within the right occipital cortex. However, there did exist significant correlations between the fractional anisotropy of the left visual cortex and nystagmus characteristics for both the left and right eye of LCA2 patients. Data are shown for 7 LCA2 patients treated in the right eye (9 of 10), with nystagmus information missing for 2 patients.

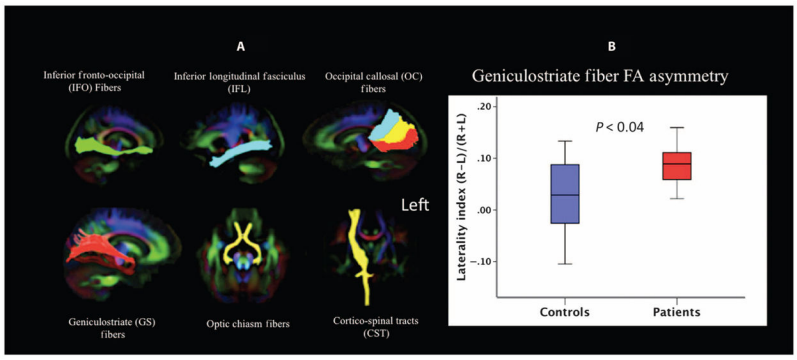

Fig. 5. DTI fiber tractography

(**A**) Using DTIStudio tractography software and a population-specific template, major fiber tracts connecting the occipital cortex to the rest of the brain such as the inferior fronto-occipital fibers, inferior longitudinal fasciculus, occipito-callosal, and geniculostriate fibers, as well as chiasm tracts, were extracted bilaterally. Subsequent to extractions, fiber bundles were superimposed on the color fractional anisotropy template image. The template image is shown in radiological convention (right brain side is shown on the left). Following Dougherty *et al*. (20), the occipito-callosal fibers were extracted by placing three regions of interest in the upper, middle, and lower areas of the inferior portion of the splenium to extract tracts that ended in dorsal V3 visual areas (blue), dorsal and ventral V1 and V2 areas (yellow), and ventral V3 and V4 areas (red). In addition to vision-related tracts, bilateral corticospinal tracts were extracted as nonvision control fibers. Tractography analyses of all of these tracts showed no difference between the LCA2 patients and sighted controls except for the geniculostriate fibers. As shown in Table 4, the averaged fractional anisotropy along the right geniculostriate fibers for the LCA2 patients did not differ from the control group ($P = 0.389$). However, tractography results showed significantly decreased fractional anisotropy along the left geniculostriate fibers ($P = 0.0045$). (**B**) Laterality indices (R-L) for the average fractional anisotropy along the left and right geniculostriate fibers for LCA2 patients and sighted controls were evaluated. The laterality index used was: (right geniculostriate average fractional anisotropy − left geniculostriate average fractional anisotropy)/(right geniculostriate average fractional anisotropy + left geniculostriate average fractional anisotropy). LCA2 patients showed much higher average fractional anisotropy values for the right geniculostriate fibers, and their laterality index (red bar) significantly ($P < 0.04$) differed from matched sighted controls (blue bar).

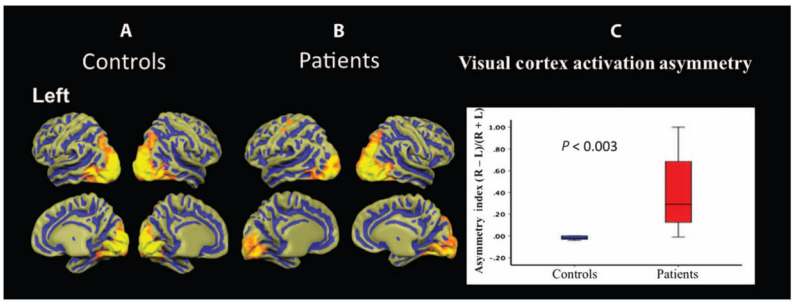

Fig. 6. Group-averaged fMRI results

(**A** and **B**) Group-averaged fMRI results of the right eye in response to high-contrast checkerboard stimuli (19) for sighted controls and LCA2 patients are depicted in (A) and (B), respectively. Cortical activations are presented on the brain atlas, which is shown in the neurological convention (left cortex depicted on the left). A symmetrical distribution of activation in both hemispheres for sighted controls as opposed to a clearly asymmetric activation distribution for LCA2 patients is shown. (**C**) The cortical activation laterality index (right total visual cortex activation volume − left visual cortex activation volume)/(right total visual cortex activation volume + left total visual cortex activation volume) is significantly larger ($P < 0.003$) for LCA2 patients compared to sighted controls.

Table 1

LCA2 patient demographics.

Demographics	Sighted controls	LCA2 patients	Statistics
n	11	10	
Male	8	6	Fisher's exact = 0.93
Average age (years)	24.37 (11.77)	23.89 (12.32)	*T* test > 0.83
Age range (years)	9.50–46.24	9.08–44.75	
Right-handed	11	9	Fisher's exact = 0.48
Average time between gene therapy and imaging	N/A	2.09 (1.11)	

Table 2
Cluster size and locations for diffusion results

Size and center of mass coordinates of the fractional anisotropy, mean diffusivity, and radial diffusivity for clusters extracted from voxel-based analyses of diffusion maps in the coordinate system of the MNI template.

Cluster locations	MNI coordinates			Cluster size (number of voxels)
Fractional anisotropy	***x***	***y***	***z***	
Left visual cortex (BA-18)	−6	−103	−5	1824
Right visual cortex (BA-17)	19	−80	5	1580
Left visual cortex (BA-17)	−3	−88	1	1448
Right visual cortex (BA-18)	24	−102	−2	378
Right visual cortex (BA-19)	43	−80	−2	343
Splenium of corpus callosum	7	−34	12	100
Radial diffusivity				
Left visual cortex (BA-17)	−12	−81	13	1495
Right visual cortex (BA-18)	7	−81	−1	813
Right visual cortex (BA-17)	10	−79	7	136
Left visual cortex (BA-17)	−2	−82	7	100
Mean diffusivity				
Right visual cortex (BA-19)	20	102	−3	601
Left visual cortex (BA-17)	−6	−94	3	540
Right visual cortex (BA-17)	11	−72	6	138
Left visual cortex (BA-17)	−2	−80	12	120
Left visual cortex (BA-19)	−32	−86	17	118

Table 3

Quantification of diffusion results

Average values for the fractional anisotropy, radial diffusivity, and mean diffusivity for the significant clusters listed in Table 2. These clusters were identified from the voxel-based analyses of diffusion maps of the LCA2 patients and sighted controls registered to the MNI template.

Cluster location	LCA2 patients	Sighted controls
	Average fractional anisotropy (SD)	Average fractional anisotropy (SD)
Right occipital	0.202 (0.018)	0.260 (0.022)
Left occipital	0.199 (0.024)	0.252 (0.025)
Splenium	0.660 (0.034)	0.711 (0.028)
	Average radial diffusivity (SD) (10^{-6} s/mm^2)	Average radial diffusivity (SD) (10^{-6} s/mm^2)
Right occipital	743.0 (38.6)	679.5 (27.2)
Left occipital	822.0 (48.8)	730.9 (43.1)
	Average mean diffusivity (SD) (10^{-6} s/mm^2)	Average mean diffusivity (SD) (10^{-6} s/mm^2)
Right occipital	816.0 (39.5)	757.3 (36.4)
Left occipital	860.0 (47.8)	783.0 (42.3)

Table 4

Fiber tractography results

Statistical comparison of average fractional anisotropy measurements for the right and left geniculostriate fibers for LCA2 patients and sighted controls.

Average fractional anisotropy	Groups	Mean	SD	*P*
Right geniculostriate	Sighted controls	0.417	0.036	0.389
	LCA2 patients	0.413	0.019	
Left geniculostriate	Sighted controls	0.397	0.041	0.0045
	LCA2 patients	0.346	0.045	

Table 5
Comparison of cortical activation in LCA2 patients and sighted controls

Statistical comparison of the total volume of cortical activation distributed within the right and left visual cortices between LCA2 patients and sighted controls resulting from the stimulation of the subjects' right eye only.

Cortical activation	Groups	Mean ($mm^{3)}$	SD ($mm^{3)}$	*P*
Right occipital lobe	Sighted controls	29,415	14,682	0.32
	LCA2 patients	22,129	13,254	
Left occipital lobe	Sighted controls	30,141	14,672	0.05
	LCA2 patients	15,143	13,348	